

INFLUENCE OF ANNEALING CONDITION AND COLD-ROLLING REDUCTION ON TEXTURE FORMATION IN AN Al-Mg-Si ALLOY

*R. Akiyoshi¹, S. Kang¹, H. Shishido¹, K. Ihara¹, and Y. Takaki²

¹*Kobe Steel, LTD., Moka, Tochigi, Japan*

(*Corresponding Author: akiyoshi.ryutaro@kobelco.com)

²*Kobe Steel, LTD., Shinagawa-ku, Tokyo, Japan*

ABSTRACT

Tensile tests and scanning electron microscopy-electron backscattered diffraction (SEM-EBSD) analysis were performed in an Al-Mg-Si alloy to clarify the effect of annealing and cold-rolling reduction on the texture formation. The hot-rolled specimens were cold-rolled with the reduction of 58-75% (CR1), followed by annealing at 773 K for 5 min (IA). The secondary cold-rolling (CR2) for the IA specimens with the reduction of 33-66%, followed by the solution heat treatment (ST), were performed. Focusing on the CR1 and CR2 specimens, the average r -values increased with higher primary and lower secondary cold-rolling reduction, respectively. This was considered to be due to the increase of r -values measured in the direction of 45 degree with respect to rolling direction, caused by the formation of the β -fiber components (Brass $\{011\}\langle 211\rangle$, Copper $\{112\}\langle 111\rangle$ and S $\{123\}\langle 634\rangle$) with high density. Based on the texture analysis of annealed specimens it was suggested that the high density of the β -fiber components after IA and the small amount of stored strain energy of CR2 introduced by the lower cold-rolling reduction remained the β -fiber components even after solution treatment.

KEYWORDS

Intermediate annealing, Cold-rolling reduction, Cube orientation, β -fiber component

INTRODUCTION

Al-Mg-Si alloys have been applied to automobile body applications, due to their excellent paint-bake hardening (age-hardening) and corrosion resistance compared to other aluminum alloy. On the other hand, the mechanical properties and deep drawability of Al-Mg-Si alloys are inferior to those of steels. Thus, it is important to improve the mechanical properties and deep drawability in order to expand the application components.

One of the best methods to improve the deep drawability is to increase the Lankford coefficient (r-value). Previous studies reported that the increase of the average r-value (\bar{r}) improves the deep drawability. The relationship between the r-value and texture of the alloy is also well known. Inoue *et al.* reported that the β -fiber components, such as Brass ($\{011\}\langle 211\rangle$), Copper ($\{112\}\langle 111\rangle$) and S ($\{123\}\langle 634\rangle$), increase the r-value measured in the direction of 45° with respect to the rolling direction.

In general, the texture evolution of alloys depends on the thermo-mechanical processing, such as intermediate annealing conditions and cold-rolling reduction. Wang *et al.* investigated the influence of intermediate annealing conditions between hot-rolling and cold-rolling on the texture evolution in the Al-0.8 Mg-0.9 Si-0.5 Cu (mass %) alloy and found that the recrystallized grain orientation of the alloy after the solid-solution treatment randomizes due to the influence of intermediate annealing. Ikeda *et al.* reported that the intermediate annealing contributes to the homogenization of texture components after the solution treatment.

The relationship between the texture evolution and thermo-mechanical processing, especially the intermediate annealing, has been investigated as described above. However, the influence of the intermediate annealing conditions and cold-rolling reduction on the texture formation is not well understood. The aim of this research is to clarify the influence of annealing conditions and cold-rolling reduction on the texture evolution in an Al-Mg-Si alloy.

EXPERIMENTAL

The chemical composition and the thermo-mechanical processing flowchart of specimens in this research are shown in Table 1 and Figure 1, respectively. The specimen was cast, homogenized and hot-rolled into 6 mm thickness. No recrystallization grains were observed in the hot-rolling specimens. The hot-rolled specimens were cold-rolled by the reduction of 58–75% (CR1) and intermediate-annealed at 773 K for 5 min (IA). The secondary cold-rolling (CR2) into 1 mm thickness for the annealed specimens were performed with the reduction of 33–66%. And then, the cold-rolled specimens were solution-treated at 823 K for 15 min (ST) and quenched into water.

Table 1. Chemical composition of the alloy.

	Si	Fe	Cu	Mn	Mg	Al
mass %	1.0	0.2	0.1	0.1	0.4	Bal.
at %	1.0	0.1	0.1	0.1	0.5	Bal.

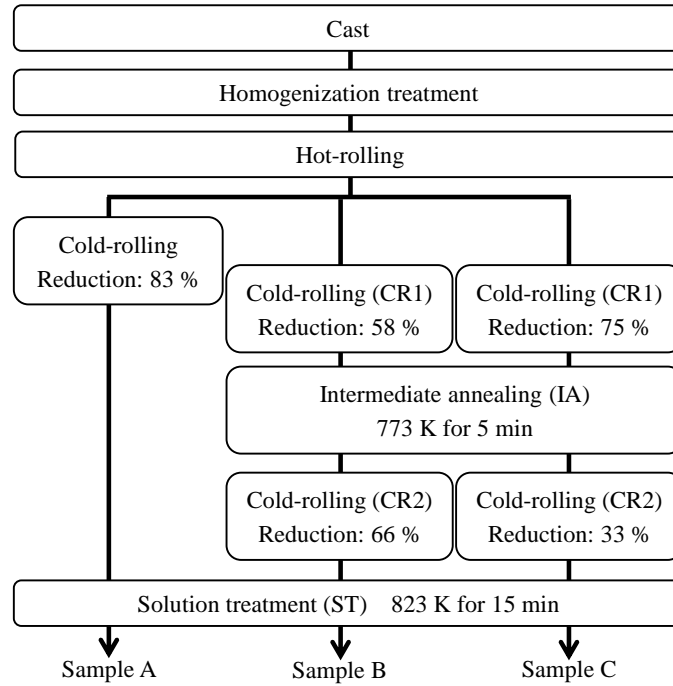


Figure 1. Flowchart of thermo-mechanical treatment of the alloy.

In order to clarify the influence of cold-rolling reduction on the r -value, the mechanical properties of specimens after ST were evaluated by using a tensile tester, Autograph AG-1 (Shimadzu, Japan) at room temperature with a strain rate of $6.25 \times 10^{-3} \text{ s}^{-1}$. The tensile test specimens with a gauge length of 80 mm and a width of 20 mm were cut from the direction of 0° , 45° and 90° with respect to the rolling direction. Each r -values were determined as the plastic strain reaching 10%. The \bar{r} value of the specimens was calculated as follows:

$$\bar{r} = \frac{r_0 + r_{90} + 2r_{45}}{4} \quad (1)$$

where, r_0 , r_{45} and r_{90} are the r -values measured in the direction of 0° , 45° and 90° with respect to the rolling direction, respectively.

An electron backscattered diffraction (EBSD) by scanning electron microscopy (SEM) was carried out to determine the crystal orientation and texture evolution of specimens. The EBSD analysis was performed by using a microscope, JSM-7100F (JEOL, Japan) equipped with orientation imaging microscopy software (TSL solutions, Japan). An orientation distribution functions (ODF) was calculated by the series expansion method under an expansion order of 22.

RESULTS AND DISCUSSION

r-Values

Figure 2 shows the r_0 , r_{45} , r_{90} and \bar{r} values of samples after ST. The \bar{r} value of sample A without IA is about 0.51. Focusing on samples B and C with IA, the \bar{r} value of sample B is almost the same as that of sample A. On the other hand, sample C is higher in the \bar{r} value than those of samples A and B. This result indicates that the \bar{r} value increases by optimizing the reduction of CR1 and CR2,

rather than only conducting with or without IA. Additionally, it is considered that the reason of the high \bar{r} value of sample C is to be higher r_{45} value by about 0.15 than that of sample B.

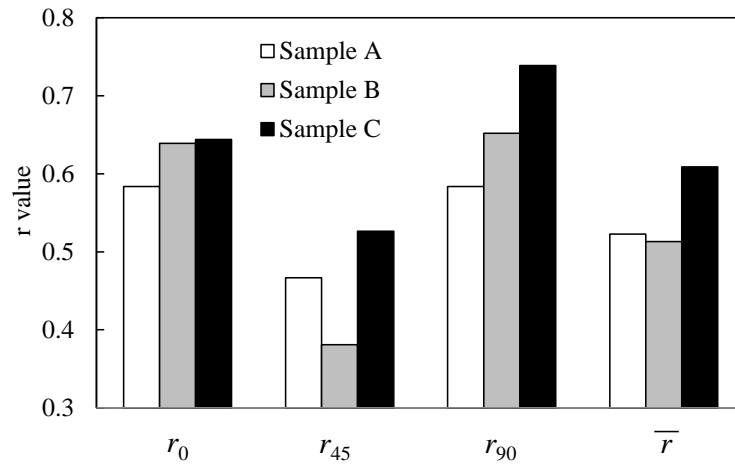


Figure 2. r-values of samples.

Texture Components of Samples after ST

The SEM-EBSD analysis of samples after ST was carried out to clarify the relationship between r-values and texture components. Figures 3 and 4 show the grain orientation distributions and ODF images obtained from the area of Fig. 3, respectively. As shown in Fig. 4(a), the main texture components in sample A is Cube and P ($\{011\}\langle 122\rangle$) orientations. Although high intensity of the Cube orientation distributed in samples B and C are seen, the β -fiber components are higher than those of sample A. It is suggested that the main texture components of samples B and C are the Cube orientation and β -fiber components. Focusing on samples B and C, in addition, sample C is higher in the intensity of the β -fiber components than that of sample B. Considering the results of previous studies, it is concluded that the formation of the β -fiber components contributes to increase the r_{45} and \bar{r} values.

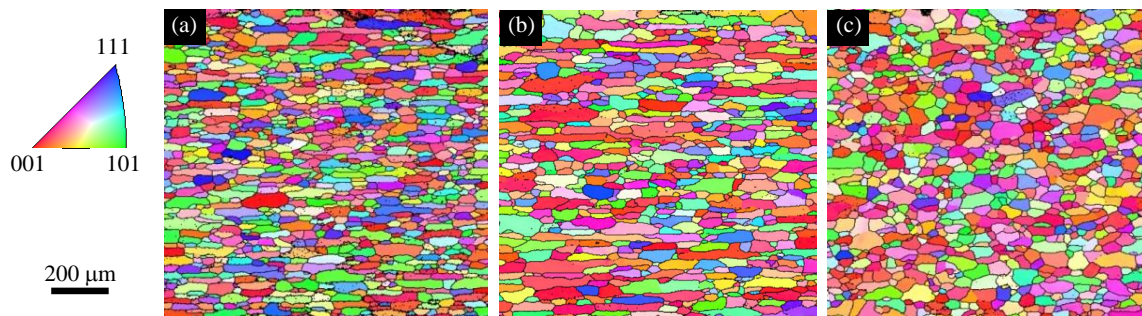


Figure 3. Crystal orientation distribution of (a) Sample A, (b) Sample B and (c) Sample C.

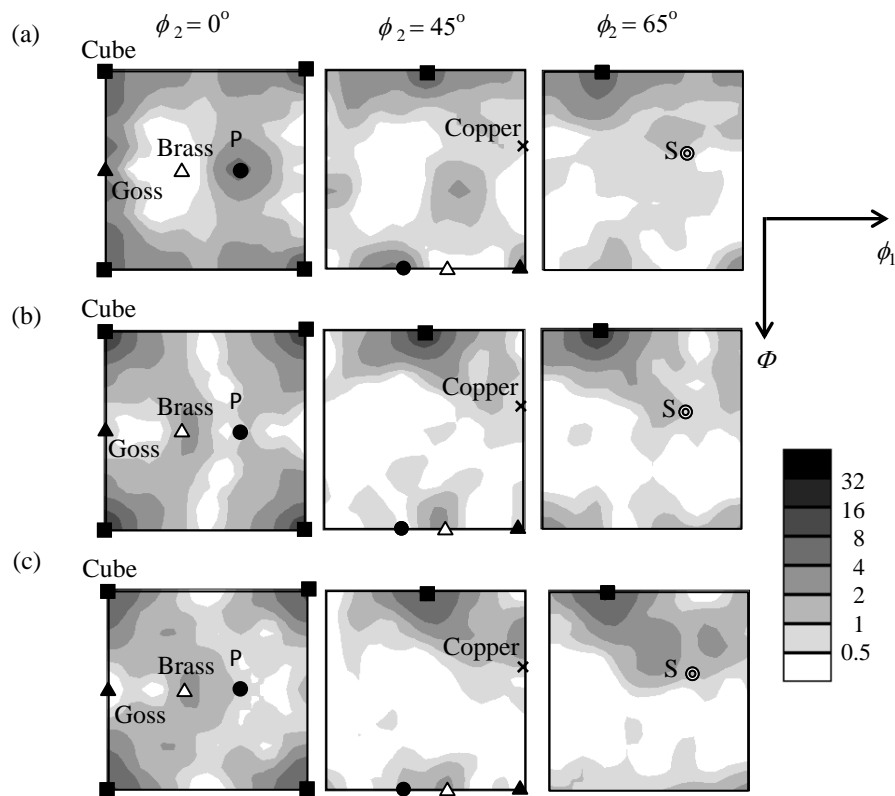


Figure 4. ODF images after ST of (a) Sample A, (b) Sample B and (c) Sample C.

Texture Formation Process

In order to find out the above texture formation process of samples B and C, the texture analysis of samples after IA and CR2 was performed. The ODF images of samples B and C after CR2 are shown in Fig. 5. Strong intensity of the Cube orientation and weak intensity of the β -fiber components are found in both samples. The intensity of the β -fiber components distributed in sample C is lower than that in sample B, which is an opposite result of samples after ST.

Figure 6 shows ODF images of samples B and C after IA. One can see the high intensity of the Cube orientation and β -fiber components, which is a similar tendency to the samples after CR2 (Figure 5). The orientation intensity in sample C is lower in the Cube orientation and higher in the β -fiber components than those in sample B. Takeda *et al.* reported that the Cube orientation density tends to decrease because of the preferential formation of the non-Cube orientation as the cold-rolling reduction becomes higher. Based on the above results and previous studies, it is considered that the amount of the Cube orientation in sample C becomes lower than that in sample B because of the preferential formation of the non-Cube orientations during IA.

The texture formation process in this research is discussed by considering above results. Figure 7 describes the texture formation process diagram of the Cube orientation and β -fiber components in samples B and C. Focusing on sample C, it is suggested that the Cube orientation density after IA is lower than that in sample B because the reduction of CR1 is high compared with sample B, and then, the Cube orientation and β -fiber components are formed by conducting CR2. Also, it is considered that the stored strain energy introduced by CR2 is lower than that in sample B because the cold-rolling reduction is low. Considering these tendency and past studies that the growth of the Cube orientation is accelerated by the presence of

stored strain energy and grains with β -fiber components, it is suggested the lower density of the Cube orientation and higher density of the β -fiber components in sample C after ST. To sum up the results, it is concluded that the r_{45} and \bar{r} values in sample C increase by the formation of the β -fiber components after ST, although the β -fiber components are low after CR2.

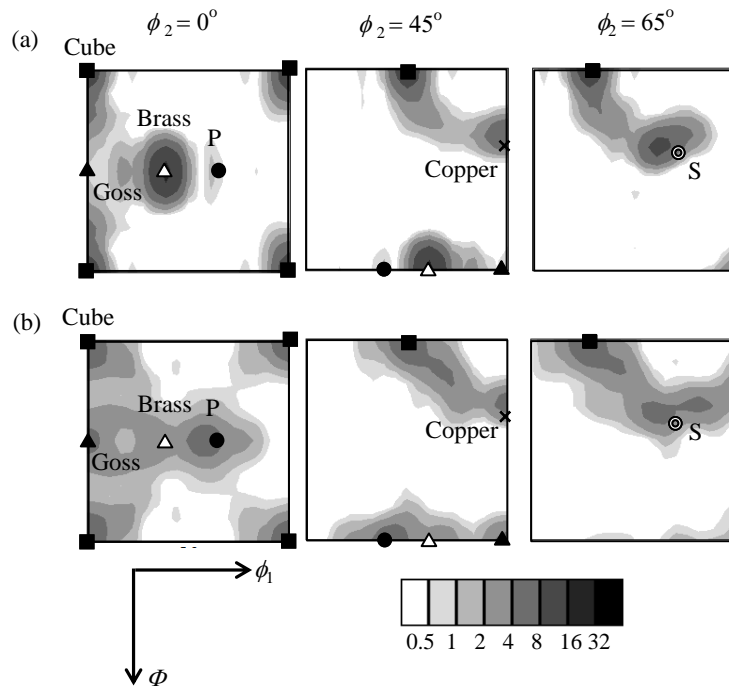


Figure 5. ODF images after CR2 of (a) Sample B and (b) Sample C.

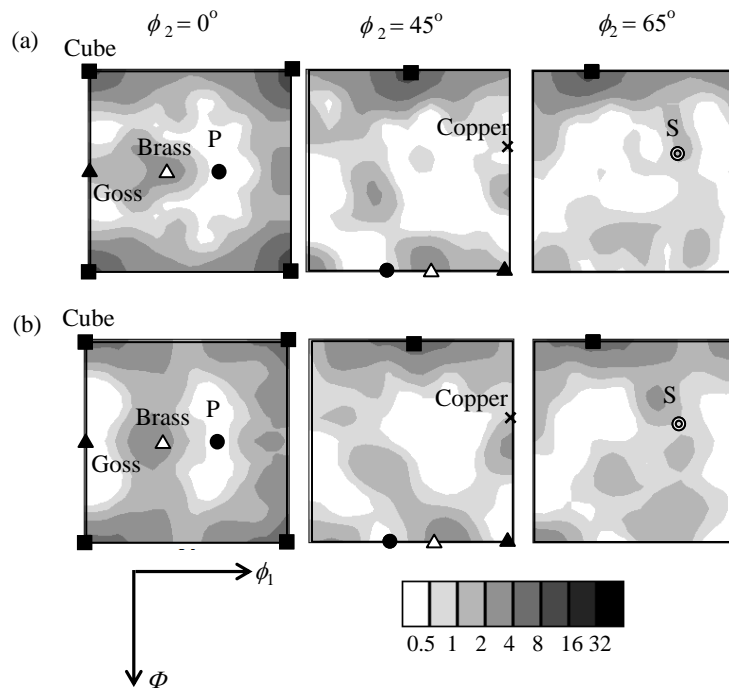


Figure 6. ODF images after IA of (a) Sample B and (b) Sample C.

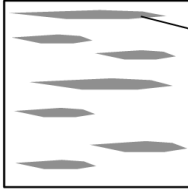
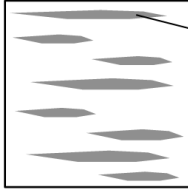
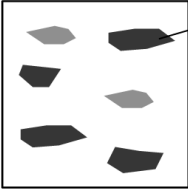
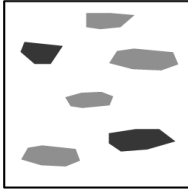
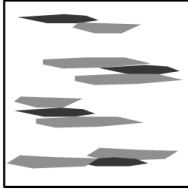
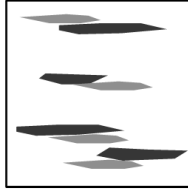
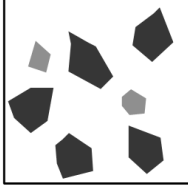
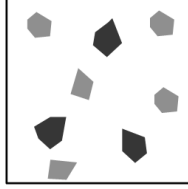
Point	Sample B	Sample C
CR1	 β -fiber components	 β -fiber components
IA	 Cube Cube density: High β -fiber density: Low	 Cube density: Low β -fiber density: High
CR2	 Stored strain energy: High Cube density: Low β -fiber density: High	 Stored strain energy: Low Cube density: High β -fiber density: Low
ST	 Cube density: High β -fiber density: Low	 Cube density: Low β -fiber density: High

Figure 7. Schematic illumination of the texture evolution of the samples B and C.

CONCLUSIONS

In this research, the influence of annealing conditions and cold-rolling reduction on the texture evolution was investigated in an Al-Mg-Si alloy. The main findings are summarized as follows:

1. The r_{45} and \bar{r} values increase when the reduction of CR1 and CR2 is higher and lower, respectively. It is assumed that the high formation amount of the β -fiber components result in the higher r_{45} values.
2. The amount of the β -fiber components in the solution-treated sample is high in the condition of higher and lower reduction of CA1 and CR2 is higher and lower, respectively. On the other hand, in the sample before ST, on the other hand, the β -fiber component density is lower than that of after ST.
3. The Cube orientation density and stored strain energy of the sample before the solution treatment are low, resulting in the low density of the Cube orientation and the preferential formation of the β -fiber components.

REFERENCES

- Hu, J., & Ishikawa, T. (1998). Texture and plastic anisotropy in aluminum alloy sheets. *Journal of Japan Institute of Light Metals*, 48(11), 540-547. <https://doi.org/10.2464/jilm.48.540>
- Ikeda, K., Miyata, Y., Yoshihara, T., Takata, N., & Nakashima, H. Effect of thermos-mechanical treatment on ridging behavior and cube-oriented grain formation process in 6111 aluminum alloy. *Journal of Japan Institute of Light Metals*, 64(8), 353-360. <https://doi.org/10.2464/jilm.64.353>
- Inoue, H., & Inakazu, N. (1993). Estimation of r-value in aluminum alloy sheets by quantitative texture analysis. *Journal of Japan Institute of Light Metals*, 44(2), 97-103. <https://doi.org/10.2464/jilm.44.97>
- Lankford, W. T., Snyder, S. C., & Bauscher, J. A. (1950). New criteria for predicting the press performance of deep drawing sheets. *Transactions of American Society for Metals*, 42, 1197-1232.
- Takeda, H., Hibino, A., & Takata, K. (2012). Effect of cold-rolling reduction on development of recrystallization textures in an Al-Mg-Si alloy. *Journal of Japan Institute of Light Metals*, 62(2), 60-66. <https://doi.org/10.2464/jilm.62.60>
- Wang, X., Guo, M., Chapuis, A., Luo, Jinru., Zhang, J., & Zhuang, L. (2015). The dependence of final microstructure, texture evolution and mechanical properties of Al-Mg-Si-Cu alloy sheets on the intermediate annealing. *Materials Science & Engineering A*, 633, 46-58. <https://doi.org/10.1016/j.msea.2015.02.029>